

Spatial structure of broad-area vertical-cavity regenerative amplifiers

T. Ackemann^{†*}, S. Barland[†], M. Cara[‡], S. Balle[‡], J. R. Tredicce[‡], R. Jäger[¶], M. Grabherr[¶], M. Miller[¶], K. J. Ebeling[¶]

[†] *Institut Non Linéaire de Nice, UMR 6618 CNRS-UNSA, 1361 Route des Lucioles, F-06560 Valbonne, France*

[‡] *Dept. de Física Interdisciplinar, Instituto Mediterráneo de Estudios Avanzados, IMEDEA (CSIC-UIB), E-07071 Palma de Mallorca, Spain*

[¶] *Department of Optoelectronics, University of Ulm, Albert-Einstein-Allee 45, D-89069 Ulm, Germany*

(Submitted to Opt. Lett. 20.1.2000)

Abstract

We investigate the spatial structure of broad-area vertical-cavity regenerative amplifiers with injection of a homogeneous beam. The emerging patterns have a dominantly six-fold rotational symmetry verifying the recent prediction of hexagons. The length scale is controllable via the detuning and follows the prediction for tilted waves.

PACS number(s): 42.65.Sf, 42.55.Px, 42.55.Sa, 42.65.Pc, 42.60.Jf

Typeset using REVTeX

*Permanent address: Institut für Angewandte Physik, Westfälische Wilhelms-Universität Münster, Corrensstraße 2/4, D-48149 Münster, Germany, E-mail: ackeman@uni-muenster.de

The spatial structure of high power, broad-area semiconductor lasers is a subject of considerable interest both from a fundamental and an application point of view (e.g. [1–4]). The strong tendency of these lasers to emit modulated states in the form of high-order modes or filaments is a beautiful example for self-organization phenomena in nonlinear optical systems but limits severely the achievable power and/or coherence. On the other hand, certain localized nonlinear states are discussed for their potential for information encoding and processing [5–7]. In particular, recent work predicts the possibility of addressable soliton-like excitations (cavity solitons) in semiconductor microcavities [8,9], which might enable new forms of all-optical, massively parallel information processing. Following the suggestion in [8], we study in a first step the spatial structure of broad-area vertical-cavity surface-emitting lasers (VCSEL) which are operated as regenerative amplifiers, i.e. biased electrically below threshold but above transparency and subjected to external injection of a homogeneous beam.

The devices under study are based on three InGaAs/GaAs quantum wells of thickness 8 nm embedded in a spacer layer with a thickness of one wavelength. The cavity is closed by Bragg reflectors with 30 stacks on the p-side and 20.5 on the n-side. A detailed description of the devices can be found in [10]. The size of the active area is defined by a thin oxide aperture (diam. 54 μm) which provides the current as well as the optical confinement. Emission takes place through the thinned, antireflection coated substrate on the n-side. This *bottom-emitting* geometry provides a better uniformity of the current and carrier distribution in the active layer than a top-emitting one [4]. Most of the devices under study were operated without prior packaging (on-wafer testing). The free running lasers start at threshold typically in a high order Laguerre-or Hermite Gaussian mode [11].

Fig. 1 shows a schematic view of the setup. A high power edge emitting semiconductor laser stabilized by feedback from an external grating serves as a master oscillator. The beam profile is symmetrized by an anamorphic prism pair, spatially filtered and injected in the VCSEL such that it fills the aperture. The maximum available power level in front of the VCSEL amounts to some mWs and is controlled by an acoustooptical modulator.

The injected beam is linearly polarized with the polarization axis coinciding with the axis of the dominating polarization component of the free-running VCSEL (however, the results are not sensitive to this choice). The VCSEL is temperature controlled and driven cw by a commercial laser diode driver in current-stabilization mode. The output light is collimated with an aspheric lens (NA 0.41). Its near field (NF) and far field (FF) intensity distributions are observed with two charge-coupled device (CCD-) cameras. Signals proportional to the spatially integrated output and injected power are obtained by focusing some fractions of the beam onto low-bandwidth photodetectors. The stability and single-mode operation of the master oscillator is checked with a plano-planar scanning Fabry-Perot interferometer. The spectral characteristics of the VCSEL emission are obtained with the help of a monochromator (resolution about 0.05 nm) and a plano-planar scanning Fabry-Perot interferometer.

In the following we will discuss the changes in the emission of the VCSEL (slave) in dependence on the wavelength of the injection at constant power level. The slave was biased at 97% of threshold but the results are not sensitive to this particular value. Fig. 2 reports the amplification factor of the total injected power. It is maximum for a slight red detuning of the master compared to the emission wavelength of the free-running laser. From this measurement one would expect the longitudinal cavity resonance of the VCSEL to be around 986 nm, a more accurate value is inferred from the measurements below. The absolute value of the amplification depends of course on the distance of the slave to threshold and the power level of the injection (Fig. 2 is taken at a power level where the amplification is already slightly saturated.) A detailed discussion is not the subject of this letter, instead we will focus on the emerging spatial structures.

If the wavelength of the master oscillator is blue detuned with respect to the cavity resonance, the emission shows distinct contributions on a ring in Fourier space which contracts if the detuning is reduced (Fig. 3h-n). The amplitude of the off-axis emission is rather small, especially far away from the resonance, therefore the far-field images are strongly overexposed at the DC-peak (most apparently in Fig. 3h), which corresponds to the amplified injected field itself. In the near field irregular modulations of low amplitude are observed

for high detuning (Fig. 3a). Reducing the detuning, the modulation depth increases and a tendency of the modulations to arrange along rings is apparent (Fig. 3b-f). The modulations within the rings increases (Fig. 3b, c) until true symmetry breaking sets in (Fig. 3c-d). The inner part of these patterns has an approximate six-fold rotational symmetry (Fig. 3d-f). This observation verifies the prediction of hexagons [8], though there is apparently still some influence from the circular boundary conditions. However, the patterns are certainly different from Hermite-/Laguerre-Gaussian modes or frequency-locked superpositions of a few of them. Moving towards the longitudinal resonance, the near field patterns become coarser until the length scale of the pattern is of the order of the laser aperture and typically a single bright peak survives (Fig. 3g). Its position within the aperture varies from device to device. The increase in modulation depth and the coarsening reflects the increase in amplitude and the reduction in transverse wavenumber described before for the far field patterns. Increasing the injection wavelength further, the interaction between the injected light and the cavity is lost and the reflected intensity distribution is essentially the master alone.

The spatial length scale of the patterns does not depend significantly on the beam parameters of the injected beam as long as it is enlarged. Tight focusing however produces an excitation of a broad spectrum of transverse wavevectors. For a homogeneous injection, the square of the transverse wavevector depends linearly on the detuning (Fig. 4). Such a scaling is expected for diffractive patterns in a plano-planar cavity. Concretely, one finds that the transverse wavevector q of the resonant plane waves with the wavelength λ_{inj} in a plano-planar cavity is given by

$$q^2 = 8\pi^2 n_0^2 (\lambda_0 - \lambda_{inj}) / \lambda_0^3, \quad (1)$$

where λ_0 denotes the vacuum wavelength of the longitudinal cavity resonance and n_0 the refractive index. Fitting the observed dependence of q to a straight line one obtains 986.09 nm as the intercept with $q = 0$, which should denote the position of the longitudinal resonance. This is in accordance with the expectation from Figs. 2 and 3. Using this value and $n_0 = 3.5$ as an average refractive index for the semiconductor material one obtains the

solid line in Fig. 4 demonstrating that not only the scaling but also the absolute value of the wavevector is reproduced rather accurately by the theory.

The off-axis waves are emitted spontaneously (cf. the discussion below) since they are favored to the off-resonance injected on-axis wave by the resonance properties of the cavity. This is the origin of the modulational instability predicted in [8]. Theoretically, the importance of the off-axis or *tilted wave* mechanism for the length scale selection in nonlinear plano-planar cavities has been established years ago (cf. e.g. [12–14]) but experiments were lacking due to the difficulties to achieve high Fresnel numbers in plano-planar cavities. Also the recent demonstration of tilted wave emission in a free-running VCSEL did not give an explicit measurement of the transverse wavevector in dependence on the detuning [3].

However, contrary to the expectation [9] a distinct threshold for the appearance of the off-axis wavevectors is not observed. This is probably due to linear scattering phenomena which seed a nonvanishing amplitude for the high transverse wavevectors already below the deterministic threshold and thus will wash it out. I.e., the boundary conditions do not support a true homogeneous state. Nevertheless, the resonance condition will still govern the length scale selection as long as the injection in nonresonant modes is not too high (see the discussion for the focused injection above). Furthermore, if the amplitude in the high q grows large, nonlinear coupling between them takes place which is responsible for the emergence of a macroscopic symmetry which is the one favored by the nonlinear dynamics (hexagonal in this case, [8,9]). Possible sources of this scattering are the boundaries (e.g. of the light in the beam wings at the oxide layer), irregularities in the material and/or the resonance condition or the finite spread of the wavevector spectrum of the incident beam. The relative importance of the different factors has to be addressed in future experiments.

We remark that there is optical bistability in a parameter window close to the longitudinal resonance which is however considerably narrower than predicted in [9]. This effect and its possible connection to gradient inhomogeneities in the cavity resonance [15] has also to be investigated in more detail.

T.A. gratefully acknowledges financial support from the Alexander von Humboldt-

Stiftung. The work was supported by the PIANOS project of the European Union (project no. 28235). We thank our partners for many discussions on the subject.

REFERENCES

- [1] R. J. Lang *et al.*, Appl. Phys. Lett. **62**, 1209 (1993).
- [2] I. Fischer, O. Hess, W. Elsässer, and E. Göbel, Europhys. Lett. **35**, 579 (1997).
- [3] S. Hegarty, G. Huyet, J. G. McInerney, and K. D. Choquette, Phys. Rev. Lett. **82**, 1434 (1999).
- [4] R. Michalzik, M. Grabherr, and K. J. Ebeling, Proc. SPIE **3286**, 206 (1998).
- [5] G. S. McDonald and W. J. Firth, J. Opt. Soc. Am. B **7**, 1328 (1990).
- [6] N. N. Rozanov, Proc. SPIE **1840**, 130 (1991).
- [7] *Self-organization in optical systems and application in information technology*, Vol. 66 of *Springer Series in Synergetics*, edited by M. A. Vorontsov and W. B. Miller (Springer, Berlin, Heidelberg, 1995).
- [8] M. Brambilla *et al.*, Phys. Rev. Lett. **79**, 2042 (1997).
- [9] L. Spinelli *et al.*, Phys. Rev. A **58**, 2542 (1998).
- [10] M. Grabherr *et al.*, IEEE Photon. Tech. Lett. **10**, 1061 (1998).
- [11] T. Ackemann *et al.*, (1999), submitted to J. Opt. B: Quantum Semiclass. Opt.
- [12] P. Jakobsen, J. Moloney, A. Newell, and R. Indik, Phys. Rev. A **45**, 8129 (1992).
- [13] K. Staliunas, Phys. Rev. A **48**, 1573 (1993).
- [14] W. J. Firth and A. J. Scroggie, Europhys. Lett. **26**, 521 (1994).
- [15] S. Coen, M. Tlidi, P. Emplit, and M. Haelterman, Phys. Rev. Lett. **83**, 2328 (1999).

FIGURES

FIG. 1. Scheme of experimental setup: EGTL external grating tunable laser, OD optical diode, AOM acoustooptical modulator, ANP anamorphic prism pair, SF spatial filter, $\lambda/2$ half-waveplate, LP linear polarizer, CCD charge-coupled device camera, SFPI scanning Fabry-Perot interferometer, MO monochromator, D1, D2 photodetectors. The black line denotes the beam of the master oscillator, the grey one the beam emitted by the VCSEL, respectively the part of the master reflected at the input facet.

FIG. 2. Amplification of the total injected power in dependence on the injection wavelength for constant injected power. The wavelength of the free-running VCSEL at threshold is denoted by the solid vertical line. The distance between different points is about 54 GHz and is given by the free spectral range of the internal cavity of the master laser diode.

FIG. 3. Spatial structure in dependence on the injection wavelength. The two upper rows display the near field, the two lower rows the corresponding far field images. The dynamic range of each of the images is optimized for maximum contrast, therefore a comparison of the absolute intensity level in different images is not possible. The frame size of the near field images is $40 \times 40 \mu\text{m}^2$.

FIG. 4. Square of transverse wavevector in dependence on the injection wavelength. The solid line marks the prediction from Eq. 1.

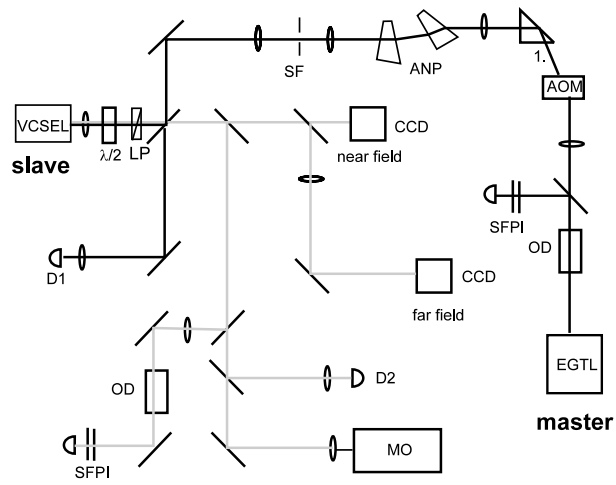


Fig. 1 of Ackemann et al.: Spatial structure of vertical-cavity amplifiers

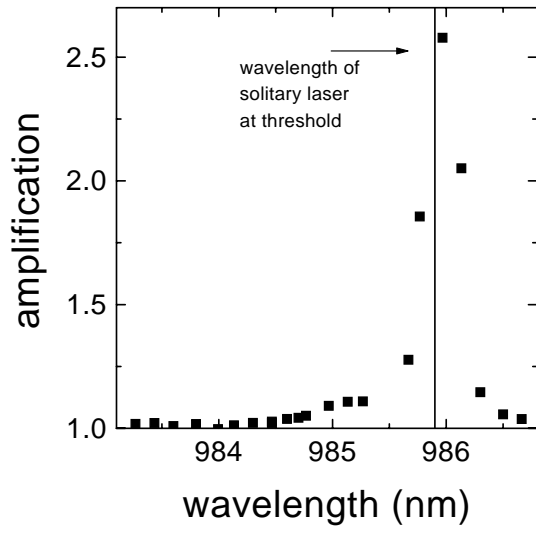


Fig. 2 of Ackemann et al.: Spatial structure of vertical-cavity amplifiers

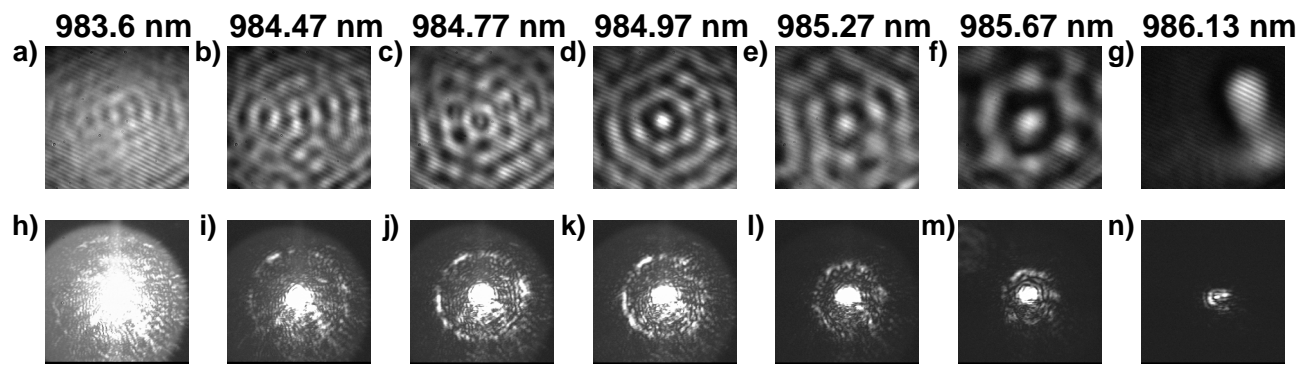


Fig. 3 of Ackemann et al.: Spatial structure of vertical-cavity amplifiers

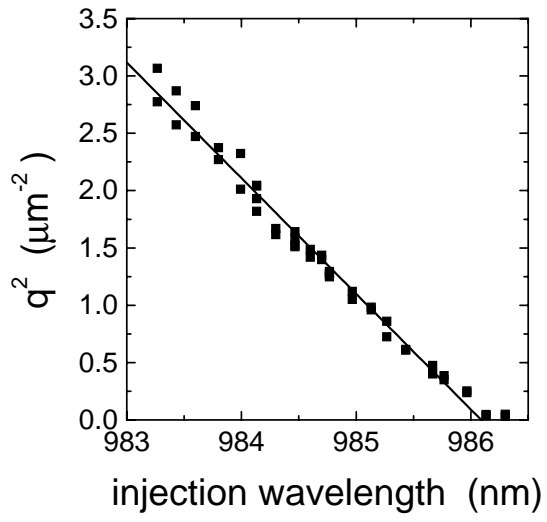


Fig. 4 of Ackemann et al.: Spatial structure of vertical-cavity amplifiers